IEEE Access
Multidisciplinary | Rapid Review | Open Access Journal

Received August 9, 2019, accepted August 20, 2019, date of publication August 27, 2019, date of current version September 11, 2019.

*Digital Object Identifier 10.1109/ACCESS.2019.2937895*

# The Modulation Technology of Chaotic Multi-Tone and Its Application in Covert Communication System

**YONGQING FU, SHENGNAN GUO, AND ZHIXIN YU**
College of Information and Communication Engineering, Harbin Engineering University, Harbin 150001, China
Corresponding author: Shengnan Guo (guoshengnan@hrbeu.edu.cn)

**ABSTRACT** With the development of communication countermeasure technology, the existing communication mode is exposed to intercept or decipher in the covert transmission of information. Therefore, the development of a new concept and principle covert communication technology with low interception probability and anti-non-cooperative demodulation has drawn increasing attention. In this treatise, we propose a chaotic multi-tone modulation and demodulation technology thus present a method to construct the covert communication system. The technology constructs chaotic multi-tone sets to express the baseband information with the multi-value mapping based on the dynamics principle, which can express the same baseband information with different multi-tone groups. Signal modulation is accomplished by combining frequency hopping and baseband information scrambling technology. Multi-value mapping is adopted to complete chaotic multi-tone modulation. Specifically it has strong information concealment and anti-non-cooperative demodulation characteristics. In order to solve the demodulation problem of the cooperative party, we present a demodulation scheme based on chaotic multi-tone and provide a complete chaotic multi-tone communication system construction scheme. Simulation results verify the performance of the proposed method.

**INDEX TERMS** Chaotic multi-tone, covert communication, low interception probability, information concealment.

## I. INTRODUCTION

At present, convert communication technologies mainly include spread spectrum communication, mixed spread spectrum communication, chaotic communication and encrypted communication [1]–[4]. Spread spectrum communication reduces the power spectrum density of useful signals in the channel through expanding baseband signal to a wide frequency band with pseudo-random code to realize signal covert transmission. The common spread spectrum communication is mainly composed of direct sequence spread spectrum (DS), frequency hopping (FH), and time hopping (TH). Direct Sequence Spread Spectrum (DSSS) is used in mobile communications but the spread spectrum sequence of different users in asynchronous network is not completely orthogonal thus causing multi-path interference. Nowadays, spread spectrum communication mode combined with orthogonal frequency division multiplexing technology (OFDM) is used to reduce multi-path interference [5]. However, because of its sensibility to phase noise and carrier frequency-offset, the reliability of the system becomes worse at low sinal-to-noise ratio(SNR). In addition, DSSS code can be easily cracked, which leads to its limitations in the application of covert communication. Mixed spread spectrum communication usually adopts a combination of one or several spread spectrum communication modes, which has higher anti-interference and concealment performance than conventional spread spectrum communication [6], [7]. Joint Tactical Information Distribution System (JTIDS) signal is a typical application combining DS, FH and TH technology [8]. DS is mainly used to reduce the power spectral density of signals. FH is mainly used to avoid interference. And TH is used to destroy the synchronization of data frames by non-cooperative parties in order to protect communication data from being intercepted by the enemy. As current broadband receiver, machine learning and data tracking technology become more and more mature, frequency hopping patterns are easy to be deciphered. In addition, the signal has poor

The associate editor coordinating the review of this article and approving it for publication was Xueqin Jiang.

error code performance at low SNR. Therefore, the research on the feasibility of usage of covert communication methods has been intensely discussed.

Chaotic communication mainly can be divided into chaos masking, chaotic modulation technology and chaos shift keying technology. The complexity of chaotic waveform and the uniformity of power spectrum reduce the probability of signal interception. However the performance of this communication method mainly depends on the realization of chaotic system synchronization [9]–[11]. While the channel noise increases the difficulty of the chaotic system synchronization the cooperative communication is difficult to achieve. Encrypted communication mainly ensures the security of information transmission by encrypting baseband information [12]. Common encryption methods include chaotic scrambling, DES(Data Encryption Standard), AES(Advanced Encryption Standard), etc., [13], [14]. This encryption method often combines with other hidden communication methods to reduce the detection probability of communication signals.

Note that the spread spectrum communication and chaotic communication that the spread spectrum communication can effectively improve the signal concealment and reduce the probability of signal interception. It is necessary to generate frequency hopping patterns in a way with higher predictive difficulty to fight against existing identification and decoding technologies effectively. Chaotic communication still needs to find a larruping and more robust communication scheme to improve the reliability of cooperative communication [15]–[18]. To solve the problem of poor reliability, easy interception and deciphering of existing covert communication systems at low SNR [19]–[21], this paper proposes modulation and demodulation method to convey baseband data information with the mathematical characteristics of multi-tone which realizes multi-valued maps between baseband data and multi-tone frequency groups. In order to achieve better hidden communication performance, we use the discrete chaotic sequence mapping method to select multi-tone frequency groups. Besides, this method also introduces channel hopping technology between adjacent symbols to enhance the anti-interception performance of the communication system. Each hop contains multiple single audio frequencies which vary according to the chaotic law, so it can reinforced the difficulty of third-party decoding. After completing the modeling of chaotic multi-tone modulation and demodulation algorithm, this paper provides a complete communication system implementation scheme and analyzes the system reliability under the simulation environment.

The rest of paper is organized as follows. In Section II, we introduce the chaotic system of multiple tones modulation and demodulation method and way to apply the dynamics principle to generate discrete chaotic sequence. Section III proposes the design scheme of chaotic multi-tone covert communication system. Section IV evaluates the anti-interference performance of the system. Finally, Section V concludes this paper.

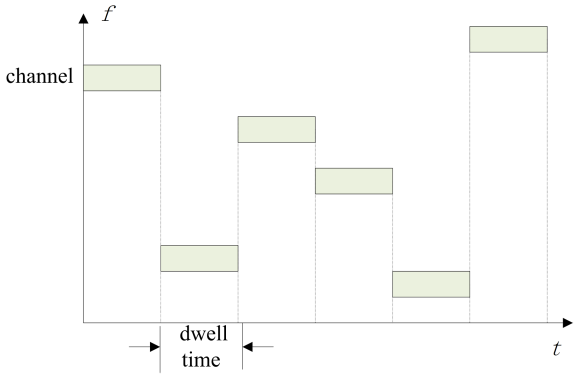


**FIGURE 1.** Schematic diagram of channel hopping.

## II. THE MODULATION AND DEMODULATION TECHNOLOGY OF CHAOTIC MULTI-TONE

The chaotic multi-tone system transmits the baseband data information through the statistical characteristics of the multi-tone frequency group with each symbol mapping to several multi-tone frequency group. In order to reduce the mutual correlation between adjacent codes and multi-tone frequency groups, this paper uses quantized chaotic discrete sequences and multi-tone frequency groups to construct the mapping relationship. Because the multi-tone frequency groups corresponding to each symbol have chaotic characteristics, it is called chaotic multi-tone.

### A. CHAOTIC MULTI-TONE MODULATION AND MATHEMATICAL MODELING

In order to improve the concealment of communication waveforms, the symbol dynamics principle is adopted to map between the multi-tone frequency set and baseband data. As a special multi-carrier transmission mode, according to the principle of anti-channel interference in frequency division multiplexing communication system [22], the chaotic multi-tone scheme is designed to reduce the frequency correlation between the adjacent symbols in the baseband. Hence the channel between adjacent symbols adopts hopping mode as shown in FIGURE.1.

In FIGURE.1, the dwell time of each hop is $g(t)$.

$$g(t) = \begin{cases} 1, & t \in [(i-1)T_b, iT_b) \\ 0, & \text{others} \end{cases} \tag{1}$$

$T_b$ is the time length of code elements. Assuming that the baseband data is a binary symbol sequence, the multi-frequency group in each hop carries one bit of information. To avoid channel interference and improve waveform concealment, the channels of adjacent symbols maintain a certain frequency interval.

Chaotic multi-tone signal can be expressed as:

$$s(t) = g(t)\, s_i(t) \tag{2}$$

$s_i(t)$ is the signal within the time of each code elements. Supposing the base-band data is $D = \{d_1, d_2, \cdots d_n\}$,

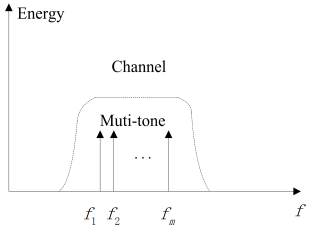


**FIGURE 2.** Chaotic multi-tone in a single channel.

and each baseband data can be represented in the channel as:

$$s_i(t) = \sum_{j=1}^{m} a_m \cos\left(2\pi f_{(i,j)} t + \varphi\right) \tag{3}$$

In formula (3), $m$ is the number of single tone in each channel, and $a_m$ is the amplitude. Where, $f_{(i,j)}, j = 1, 2, \cdots, m$ is the single-tone frequency used to transmit baseband information $d_i$. The frequency composition of signals in each channel is depicted in FIGURE.2.

FIGURE.2 shows the multi-tone frequency in each symbol channel. Assumed that the baseband channel frequency band range is $f_L$-$f_H$, and the bandwidth is:

$$B_w = f_H - f_L \tag{4}$$

Considering each $X$ Hz as a channel and the number of channels is $L = {}^{B_W}/_{X}$, $L \gg 1$. It is assumed that the frequency interval between each frequency point in each channel is $\Delta f$ Hz, and the intermediate frequency of the channel $f_{o,i'}, i' = 1, 2, \ldots, L$ serves as the reference frequency. Accordingly, the number of single audio points available in each channel can be expressed as:

$$n = {}^{X}/_{\Delta f} - 3, \quad n \gg 1 \tag{5}$$

The number of $m$ single tone frequencies are arbitrarily selected from the number of frequency points as a multi-tone frequency group. The number of multi-tone frequency sets in each channel is:

$$N = C_n^m = \frac{(n-1)(n-2)\cdots(n-m)}{(m)(m-1)\cdots 1} \tag{6}$$

According to the combination coding theorem, we can take the combination of $m$ elements from the number of $n$ different elements. When the combined elements are $f_1, f_2, \cdots, f_m$, the combination number based on the permutation is determined by the following formula:

$$N = f_m + f_{m-1} + \sum_{t=0}^{m-2} \left(C_{n-f_t}^{m-t} - C_{n+1-f_{t+1}}^{m-t}\right), \quad f_0 = 0 \tag{7}$$

After the frequency band range corresponding to the baseband code is selected, a multi-tone frequency group can be generated in the above way. The set of multi-tone frequency groups in the $i'th$ channel can be expressed as:

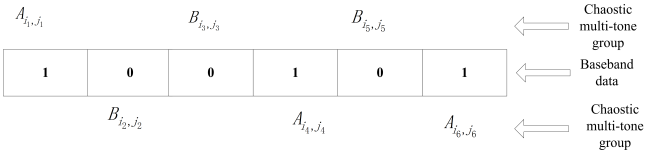


**FIGURE 3.** The relationship between the multi-tone frequency group and the baseband symbol.

$c_{i'} = \left\{c_{i',1}, c_{i',2}, \ldots, c_{i',N}\right\}$. All multi-tone frequency groups are:

$$c = \begin{bmatrix} c_{11} & c_{12} & \cdots & c_{1N} \\ c_{21} & c_{22} & \cdots & c_{2N} \\ \vdots & \vdots & \ddots & \vdots \\ c_{L1} & c_{L2} & \cdots & c_{LN} \end{bmatrix} \tag{8}$$

Further calculation of the mean of frequency points in multi-tone group can be expressed as follows: $\overline{f_{i',j'}} = \frac{1}{m}\sum_{j=1}^{m} f_j$. According to the relationship between $\overline{f_{i',j'}}$ and $f_{o,i'}$, the multi-tone frequency group can be divided into two groups. The relationship can be written as:

$$\begin{cases} \overline{f_{i',j'}} < f_{o,i'}, c_{i',j'} \in B \\ \overline{f_{i',j'}} > f_{o,i'}, c_{i',j'} \in A \end{cases} \tag{9}$$

Based on this division, multi-tone frequency sets in the *ith* channel can be expressed as: $A_{i'} = \left\{A_{i',1}, A_{i',2}, \ldots, A_{i',n_A}\right\}$, $B_{i'} = \left\{B_{i',1}, B_{i',2}, \ldots, B_{i',n_B}\right\}$. Apparently, $(A_{i'} \cup B_{i'}) \subseteq c_{i'}, n_A + n_B < N, n_A = n_B$. To unify the mapping relation, $n_1 = n_A = n_B$. Therefore:

$$A = \begin{bmatrix} A_{11} & A_{12} & \cdots & A_{1n_1} \\ A_{21} & A_{22} & \cdots & A_{2n_1} \\ \vdots & \vdots & \ddots & \vdots \\ A_{L1} & A_{L2} & \cdots & A_{Ln_1} \end{bmatrix} \tag{10}$$

$$B = \begin{bmatrix} B_{11} & B_{12} & \cdots & B_{1n_1} \\ B_{21} & B_{22} & \cdots & B_{2n_1} \\ \vdots & \vdots & \ddots & \vdots \\ B_{L1} & B_{L2} & \cdots & B_{Ln_1} \end{bmatrix} \tag{11}$$

Define the corresponding relation between baseband code and multi-tone frequency group as:

$$d_i = \begin{cases} 0, & f_{(i,j)} \in B,\ j = 1, 2, \ldots, m \\ 1, & f_{(i,j)} \in A,\ j = 1, 2, \ldots, m \end{cases} \tag{12}$$

Moreover, the relation between the definition of the multi-tone frequency group and the baseband symbol is shown in FIGURE.3. As can be seen from FIGURE.3, the baseband data 1 can be expressed by the multi-tone frequency group sets in $A$, and similarly the multi-tone frequency group sets in $B$ can express 0. Based on the above discussion, the relationship from baseband code to multi-frequency group given by formula (12) is a one-to-many multi-value mapping.

The multi-tone frequency group mapping to each symbol is selected according to the law of discrete chaotic sequence.

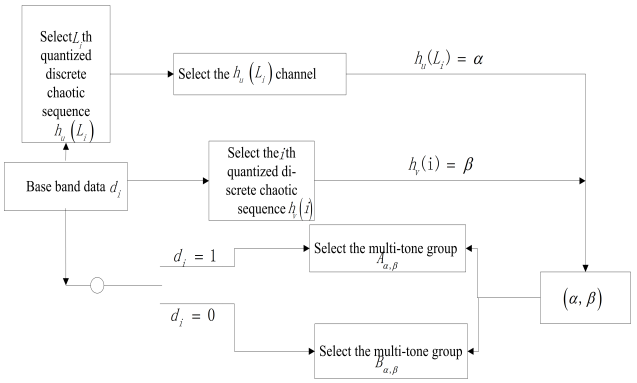


**FIGURE 4.** Schematic diagram of discrete chaotic map.

To ensure that adjacent symbols are in different channels, it is divided into two mappings. Supposed the baseband symbol to be sent is the *ith* symbol in a frame, and the channel number corresponding to the multi-tone frequency group is defined as:

$$L_i = i \bmod L + 1 \tag{13}$$

In the formula (13) $L$ is the number of channels and mod is the modular operation. According to discrete chaotic sequence, the principle diagram of selecting multi-frequency group is shown in FIGURE.4. To facilitate discussion, discrete chaotic sequences $h_u(n), n = 1, 2, \ldots, L$ and $h_v(n'), n' = 1, 2, \ldots, n_1$ used in FIGURE.4 to map channel number and chaotic multi-tone group number would be described in detail in other section.

As in FIGURE.4, we assume the base band data is $d_i$, hence, according to formula (10) select the $L_i th$ quantized chaotic sequence $\alpha$ in $h_u(L_i)$ and the $ith$ quantized chaotic sequence $\beta$ in $h_v(L_i)$. If $d_i = 1$, choose $A_{\alpha,\beta}$ as the corresponding multi-tone frequency group; otherwise, choose $B_{\alpha,\beta}$. When the frequency band range is $f_L - f_H$, the number of multi-tone frequency groups can be approximately expressed as:

$$U = \frac{(f_H - f_L)}{X} \times N \tag{14}$$

The number of total frequency points is $M_s = \frac{(f_H - f_L)}{\Delta f}$. Obviously, $U > M_s$, we can see that there is a one-to-many mapping between binary symbols and chaotic multi-tones. Moreover, there are multiplexing ways of frequency points used between different frequency groups.

Assuming that the symbol rate is $R_s$, the relationship between the symbol rate and baud rate of binary signals can be expressed as:

$$R_b = R_s \times \log_2^M, \quad M = 2 \tag{15}$$

The minimum interval of a single audio point in each multi-tone group is $\Delta f$, and when the sampling frequency is $f_s$, the number of sampling points in each symbol time is $n = {}^{T_b}/_{T_s}$, $T_b = {}^{1}/_{R_b}$. After the discrete Fourier transform, the frequency resolution is $\Delta f' = {}^{f_s}/_{n} = \frac{1}{T_b}$.

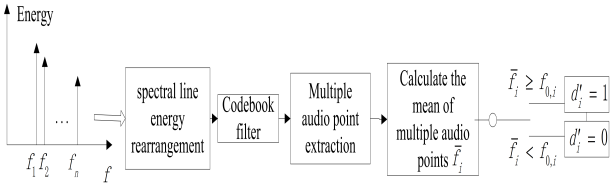


**FIGURE 5.** Schematic diagram of multi-tone demodulation algorithm.

Aiming at distinguishing each frequency point in the multi-tone group corresponding to each symbol in the demodulator, the frequency resolution should be less than the minimum interval in the multi-tone group, that is $\Delta f' < \Delta f$. Therefore the channel environment with noise, the symbol rate shall meet the following requirements:

$$R_b \gg \Delta f \tag{16}$$

After determining the baseband channel interval required to transmit the symbol and the minimum interval of single audio point in each multi-tone group, chaotic multi-tone modulation of baseband symbol can be completed by defining the symbol time according to formula (16).

### B. CHAOTIC MULTI-TONE DEMODULATION SCHEME AND MATHEMATICAL MODELING

According to the analysis of chaotic multi-tone algorithm, the key of signal demodulation lies in the effective multi-tone extraction of signals in each channel, and then the corresponding baseband code is solved. The schematic diagram of demodulation algorithm is shown in FIGURE.5.

In FIGURE.5, $\bar{f}_i$ is the mean of multi-tone frequency groups. For the *ith* symbol, $f_{o,i}$ represents the intermediate frequency of the channel in which the multi-tone frequency group is located. After FFT spectrum analysis, the signals in the channel are arranged in the order of energy from large to small. Through code-book filtering, the effective multi-tone points are extracted. Then calculate the average of the multi-audio points and compare with the center frequency of the channel to obtain the demodulation results. In a gaussian white noise channel, the signal of the *ith* symbol can be written as:

$$r_i'(t) = s_i'(t) + n(t) \tag{17}$$

$n(t)$ is the additive gaussian white noise. While the sampling period is $f_s$ and the sampled signal is:

$$r'_i(nT_s) = \sum_{j=1}^{m} a_m \cos\left(2\pi f'_{(i,j)} nT_s + \varphi\right) + n(nT_s) \tag{18}$$

Take the Fourier transform at n of (18). Then the spectrum is:

$$f_k = \sum_{i=1}^{n} r_i' e^{-j\frac{2\pi}{n}ki} = |F_k| e^{j\varphi_k} \tag{19}$$

where $k = 1, 2, \ldots, n$. Search the spectral lines of the maximum energy value successively and detect whether they

belong to the code-book until the number of $m$ bars are found. The code-book is $A \cup B$ and steps of the code-book filtering algorithm are as below:

1. Determine whether the frequency point $|F_k|$ corresponding to $f_k$ is within the code-book range $f_L - f_H$. If yes, execute next step. Otherwise, select another spectral line.
2. Determine whether the spectral is integer multiple of $\Delta f$. If yes, execute next step. Otherwise, select another spectral line.
3. Record the first line satisfying the conditions of step 1 and 2. Starting from the second line that meets the requirement. Judge whether the minimum frequency point interval is satisfied between any two adjacent lines. If so, recorded. Otherwise select another line and repeat the steps 1, 2 until $m$ bars are found.

The frequency point can be expressed as: $f'_{(i,1)}, f'_{(i,2)} \cdots, f'_{(i,m)}$. The mean of the multi-tone frequencies is $\overline{f_i} = \frac{1}{m}\sum_{j=1}^{m} f'_{(i,j)}$. The center frequency $f_{o,i}$ is obtained according to the result of spectral line identification. Finally the multi-tone demodulation judgment formula (20) is obtained by combining formula (12) and FIGURE.3.

$$d'_i = \begin{cases} 0, & \overline{f_i} < f_{o,i} \\ 1, & \overline{f_i} \geq f_{o,i} \end{cases} \tag{20}$$

### C. GENERATION OF DISCRETE CHAOTIC SEQUENCES BASED ON DYNAMICS PRINCIPLE

Among the common ways to generate discrete chaotic sequences, logistic mapping has stronger randomness, simple operation, and better performance in terms of balance and autocorrelation [22]–[25]. Without loss of generality, we choose logistic mapping as the chaos model. Logistic mapping is a one-dimensional non-autonomous discrete dynamic system evolved from the worm mouth model, and its evolution equation can be expressed as:

$$x_{n+1} = \mu x_n (1 - x_n), \quad x_n \in [0, 1], \ n = 1, 2, \cdots N \tag{21}$$

When $3.5699\cdots < \mu \leq 4$, the Logistic mapping function is in a chaotic state. In this section, $\mu = 4$. When equation (21) is implemented with precision on the computer, the discrete chaotic sequence is generated as follows: $x_L = \left\{x \,|x = n2^L, n = 0, 1, 2, \ldots, 2^L - 1\right\} \subset [0, 1)$. Discrete chaotic sequence $x^*$ can be expressed as:

$$x^*_{i+1} = G_L\left(4x_i^*\left(1 - x_i^*\right)\right) \tag{22}$$

In the equation, $x_i^* \in X_L$ is the discrete variable of the system, and $G_L$ () is the function of $floor_L$ (). According to the description of the dynamic characteristics of the controlled chaotic system in paper [25], the digital controlled Logistic mapping can be obtained as follows:

$$\begin{cases} x_{n+1} = \mu x^*_n (1 - x^*_n) + 2k_i \Delta x_i + (4 + e^c) x_i \\ x^*_n = G_L (x_i) \\ \Delta x_i = x_i - x^*_i \end{cases} \tag{23}$$

Among them, the parameter sequence of $K_i$ varies with time. For logistic system, its Lyapunov exponent is $\ln 2$ and the parameter $k_i$ range is: $(-2, 2)$. $c > 0$ is a given normal number in advance. For system (23), the calculation accuracy of $x_i^*$ and $x_i$ is controlled as $L$ and $k_i L$. And the required accuracy of calculation will increase with iteration, so it would show better dynamic properties at a lower implementation cost.

It is necessary to quantify the chaotic real value sequence to generate the discrete chaotic sequence we need, while The discrete chaotic real value sequence generated by factor (23) cannot directly correspond to chaotic multi-tone codes. There are two kinds of quantization methods, uniform quantization and non-uniform quantization. As generally used to generate uniformly distributed simulation sequences, uniform quantization is quantized by equal interval length. According to the analysis of modulation algorithm, there are $N$ multi-tone combinations in each channel. If the chaotic map interval is divided into $N$ uniformly distributed sub-intervals, each subinterval can be expressed as:

$$\Delta x_i = \left[{}^{i}\!/_{N}, {}^{(i+1)}\!/_{N}\right], \quad i = 0, 1, 2 \cdots N - 1 \tag{24}$$

If $x_n$ is in the $ith$ subinterval $\Delta x_i$, then $h_u(n) = i$. Thus a discrete sequence can be generated from the chaotic real value of $x^* = (x^*_0, x^*_1, x^*_2, \cdots, x^*_{N-1})$.

$$H_u = \{h_u(n), n = 0, 1, 2, \cdots, N - 1\} \tag{25}$$

In formula, different initial values produce different sequences. Because Logistic is a mapping with non-uniform distribution in the interval, the uniform quantization would lead to non-uniform frequency points, which does not meet the requirement of uniform concealment of signal spectrum distribution in communication countermeasure. Therefore, a non-uniform quantization method must be adopted to generate mapping sequences. Non-uniform quantization is based on adaptive selection.

For chaotic real-value sequences with non-uniform distribution with the value of chaotic sequence cannot be uniformly located in each sub-interval, it is necessary to use non-uniform quantization method to divide the mapping interval into adjacent continuous but unequal-length sub-intervals. Ordered quantization is generally used for non-uniform quantization of Logistic sequence. A new chaotic sequence is obtained by arranging $x^*_n, n = 0, 1, 2, \ldots N - 1$ in order. The order of each chaotic value in $X'$ in the original sequence $X$ is taken as a new discrete chaotic sequence. Due to discrete pseudo-random sequences obtained by quantization and judgment of chaotic sequences, each value of discrete pseudo-random sequences can be regarded as a symbol. Therefore, the order of each chaotic value in $X'$ in the original sequence $X$ is regarded as a set of symbols that conform to the chaotic law. According to the quantization method, each discrete chaotic real value can find the corresponding integer in the symbol set and then select the corresponding multi-tone frequency group as the address.

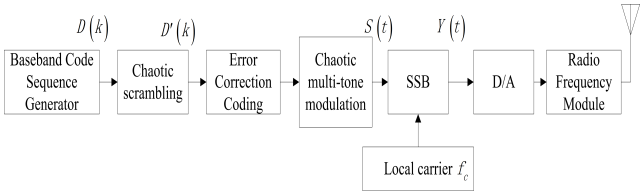


**FIGURE 6.** Transmitter structure of chaotic multi-tone covert communication system.

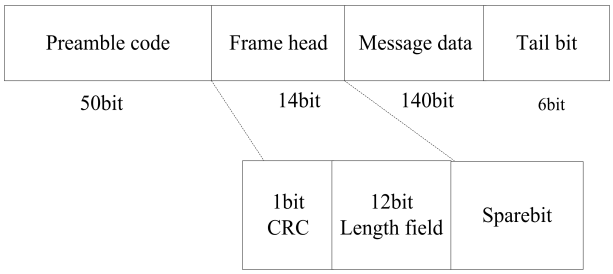


**FIGURE 7.** Frame format.

As shown in FIGURE.5, the system that chooses chaotic multi-tone groups needs to generate two discrete chaotic sequences. After determining the number of channels $L$ and the corresponding frequency combination in each channel, the discrete chaotic sequences $h_u(n), n = 1, 2, \ldots, L$ and $h_v(n'), n' = 1, 2, \ldots, n_1$ can be obtained according to the sequencing quantization method. According to the sign dynamics principle, when the initial values and the iteration times are different, the final symbol sets $h_u(n)$ and $h_v(n')$ conform to the independent distribution relationship for two groups of discrete chaotic sequences. Obviously, each address code appears only once in each cycle by ranking quantization method. Because of the dual mapping method, the final chaotic discrete sequence has higher anti-decoding ability.

## III. ARCHITECTURAL DESIGN OF REALIZATION SCHEME FOR CHAOTIC MULTI-TONE COVERT COMMUNICATION SYSTEM

### A. DESIGN OF TRANSMITTER STRUCTURE FOR CHAOTIC MULTI-TONE COVERT COMMUNICATION SYSTEM

FIGURE.6 presents the transmitter structure of the proposed system designed by the chaotic multi-tone modulation method presented in this paper.

As shown in FIGURE.6, $D(k)$ is the baseband information code, in order to improve the confidentiality and reliability of communication, we introduce chaos scrambling to baseband data and add error correction coding after processing. The scrambled symbols is $D'(k)$. After the chaotic multi-tone modulation module, the signal can be expressed as $S(t)$. Due to the low frequency of chaotic multi-tone used to carry symbol information in chaotic multi-tone system, for better transmit signals in wireless channels, it is necessary to transfer signals to high-frequency carriers for transmission, which is accomplished by single-sideband modulation. The modulated signal is $Y(t)$. Finally, the signal is sent to the RF amplifier module through D/A to complete the signal emission.

#### 1) SIGNAL MESSAGE FORMAT

To tackle the consistency of information understanding between receivers and senders, we adopt IEE802.11a standard message format [26]. Its frame structure is shown in FIGURE.7. Each frame is 210 bits, which consists of preamble, header, message data and tail bits. It can be seen from the chaotic multi-tone algorithm that the switching between neutron channels can be regarded as chaotic frequency hopping when the communication spectrum is wide. For the sake of making the receiver capture the signal accurately, chirp signal is added at the beginning of each frame of the signal as a synchronous pilot signal. The preamble serves as the basis of timing synchronization. The header consists of check bits, data length fields and standby bits. The check bits are used to check the parity of demodulated data. After the data length field is used to complete data demodulation, we can judge the validity of the received message data.

#### 2) CHAOTIC SCRAMBLING ALGORITHM

The purpose of introducing chaotic scrambling is to encrypt the message data in each frame and enhance the ability of communication system against artificial or accidental interference. Referring to the design of two-dimension code, we arrange the message data into a matrix and then rearrange the order in a chaotic way [24]. The specific scrambling algorithm is as follows: assuming the size of the original baseband matrix is $a \times b$, where $a$ is the number of frames and $b$ is the message data length of each frame. Baseband data can be represented as: $D = \{d(k) | k = 1, 2, \cdots, a \times b\}$.

According to the given Logistic mapping parameters $\mu$ and initial value $x_0$, generate a set of chaotic sequences $X = \{x(k) | k = 1, 2, \cdots, a \times b\}$ and then arrange a new sequence $X' = \{f[x(k)] | k = 1, 2, \cdots, a \times b\}$ in descending order by ranking quantization method for $X$. $f[x(k)]$ stands for scrambling rules. According to $X'$, the baseband data sequence is scrambled. For transmitter scrambling operation, it can be expressed as:

$$Z[(D(k))] = D'(k) \tag{26}$$

On the receiver side, the inverse scrambling operation is:

$$\bar{Z}\left[\left(D'(k)\right)\right] = D(k) \tag{27}$$

In the formula,

$$Z[(\bullet)] = f[D(k)] \tag{28}$$

#### 3) ERROR CORRECTION OF CODING

Error correction coding of signals is a basic way to enhance the confidentiality of communication physical layer. We establish a corresponding relationship between the information symbols and supervisory symbols to find and correct errors by adding some supervisory symbols to the transmitted information. BCH code is a complete code that

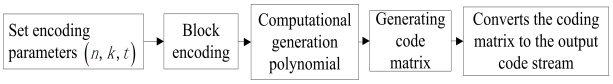


**FIGURE 8.** Coding flow.

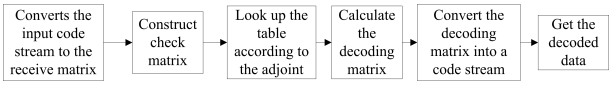


**FIGURE 9.** Decoding flow.

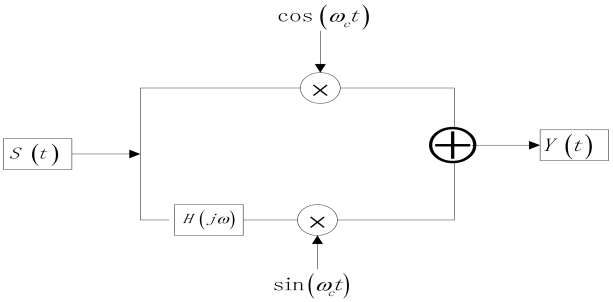


**FIGURE 10.** Implementation principle of USB modulation.

can correct multiple errors at present [28], [29]. In order to reduce the complexity of the system we use BCH code for error correction coding. When the coding parameter is $(n, k, t)$, the code length can be expressed as: $n = 2^m - 1$. In the parameter $t$ is error-correcting ability and coding efficiency is $R_c = {}^{k}/_{n}$. We uses BCH code as (7,4,1) for error correction coding. The coding flow is shown as FIGURE.8. Considering the complexity of decoding, to reduce the computation of decoding the decoding flow is shown as FIGURE.9.

#### 4) RF MODULATION OF SIGNALS

In order to modulate the chaotic multi-tone signal to the high frequency carrier and improve the efficiency of the high frequency band, this paper adopts the USB modulation mode. Its implementation principle is shown in FIGURE.10.

In FIGURE.10, $H(j\omega)$ is a Hilbert converter. The time domain expression of upper sideband amplitude modulation can be written as:

$$Y_{USB}(t) = \frac{1}{2}\left[s(t)\cos(\omega_c t) - s_h(t)\sin(\omega_c t)\right] \quad (29)$$

In the formula, $s_h(t)$ is the Hilbert transform of $s(t)$. Fourier transform is performed on the modulated signal, and the frequency domain expression is obtained as follows:

$$Y_{USB}(j\omega) = \frac{1}{2}s(j(\omega - \omega_c)) + \frac{1}{2}s(j(\omega + \omega_c)) \quad (30)$$

In the formula (30), $|\omega \geq \omega_c|$.

## IV. RECEIVER AND KEY ALGORITHMS OF CHAOTIC MULTI-TONE HIDDEN COMMUNICATION SYSTEM

FIGURE.11 shows the receiver block diagrams of the system designed by the chaotic multi-tone demodulation method presented in this paper.

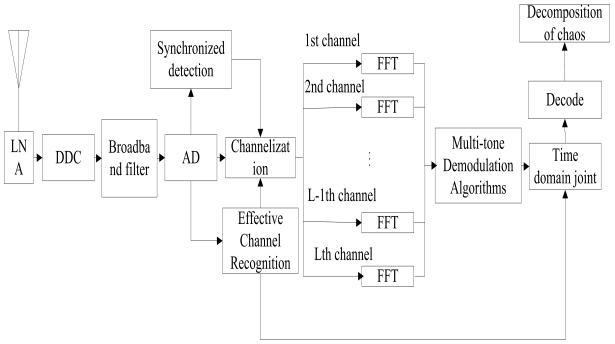


**FIGURE 11.** Receiver block diagram.

In FIGURE.11, the RF front-end circuits of LNA (Low Noise Amplifier) and broadband IF filters are in charge of the functions of signal amplification, carrier removal and suppression of out-of-band interference. Synchronization detection unit is responsible for precise time synchronization. Effective channel identification unit is responsible for channel identification of AD collected signals. The results of synchronization detection unit and effective channel identification unit are fed into the channelization unit to process the signals. After spectrum analysis of the signals in each channel, the baseband data are demodulated according to the multi-tone demodulation algorithm and spliced based on the control commands given by the channel identification unit. Then the original baseband data of covert transmission can be obtained by error correction decoding and chaotic scrambling.

#### 5) DESIGN OF SYNCHRONIZATION SCHEME FOR COMMUNICATION SYSTEM

In order to establish synchronization between transmitter and receiver, the covert communication system employs a chirp pilot signal as synchronization signal before sending data information and provides the receiver with correlation to extract the system synchronization signal. Aim to detect the communication starting point (correlation peak position) accurately and achieve lock-in synchronization from the synchronous pilot signal, we add a sweep signal to the signal starting end based on block estimation method. The signal synchronization can be achieved by the time offset obtained by two correlations at the receiver [31], [32]. To avoid the influence of synchronous pilot signal on signal reception, in the design of signal frame format, the synchronous pilot data is 50 bit. The principle of synchronous signal generation can be described as follows.

Supposing the time difference between local signal and received signal is $t_d$, after the time difference $t_d$ and doppler frequency shift $f_d$ the received pilot frequency Chirp signal $r_{syn}(t)$ can be expressed as:

$$r_{syn}(t) = {}^{\sqrt{2}}/_{2}g(t)\left[e^{j\pi u\left(t-t_d-T_p/2\right)^2} + e^{-j\pi u\left(t-t_d-T_p/2\right)^2}\right]e^{j2\pi f_d(t-t_d)} \quad (31)$$

Considering that the Chirp signal is divided into up-sweep and down-sweep signals, the local sweep signal can be expressed as:

$$\begin{cases} h_u = e^{j\pi u\left(t-\frac{T}{2}\right)^2} \\ h_d = e^{-j\pi u\left(t-\frac{T}{2}\right)^2} \end{cases} \tag{32}$$

When the local up-sweep signal is used to de-sweep the frequency, there are:

$$\begin{aligned} r_{syn}(t)\, h_u(t) &= \left[ e^{j\pi u\left(t-t_d-\frac{T}{2}\right)^2} + e^{-j\pi u\left(t-t_d-\frac{T}{2}\right)^2} \right] \\ &\quad \bullet e^{j2\pi f_d(t+t_d)} e^{j\pi u\left(t-\frac{T}{2}\right)^2} \\ &= b_u(t) + e^{j2\pi(f_d-ut_d)t} e^{j\theta} \end{aligned} \tag{33}$$

Similarly, when the local down-sweep signal is used to de-sweep the frequency, it can be expressed as:

$$\begin{aligned} r_{syn}(t)\, h_d(t) &= \left[ e^{j\pi u\left(t+t_d-\frac{T}{2}\right)^2} + e^{-j\pi u\left(t+t_d-\frac{T}{2}\right)^2} \right] \\ &\quad \bullet e^{j2\pi f_d(t+t_d)} e^{-j\pi u\left(t-\frac{T}{2}\right)^2} \\ &= b_d(t) + e^{j2\pi(f_d+ut_d)t} e^{j\theta'} \end{aligned} \tag{34}$$

In the formula (34), the first term $b_u(t)$ and $b_d(t)$ are Chirp signals with twice the sweep rate, and the second term is single-frequency signals generated by $t_d$ and $f_d$. After fast Fourier transform, the peak frequency can be obtained by calculating the peak frequency.

$$\begin{cases} f_1 = f_d - ut_d \\ f_2 = f_d + ut_d \end{cases} \tag{35}$$

According to formula (35), the signal delay can be calculated and thus the time synchronization of communication system is completed.

### 6) EFFECTIVE CHANNEL RECOGNITION

Previous analysis has shown that the chaotic multi-tone communication system presented in this paper can be regarded as a frequency hopping communication system based on a subset of multi-tone rates. Therefore, after signal synchronization, we should first consider how to roughly estimate the channel of each symbol signal in a larger acquisition range. Secondly, noted that the subsequent channelization and spectral analysis processing cannot distinguish the time-domain information of the signal, it is necessary to mark the time-domain information of the signal while identifying the channel. In this section, we use time-frequency analysis combined with image edge detection to identify the channel of the signal effectively [30]–[33]. As a chaotic multi-tone modulation signal, each single tone can be regarded as a result

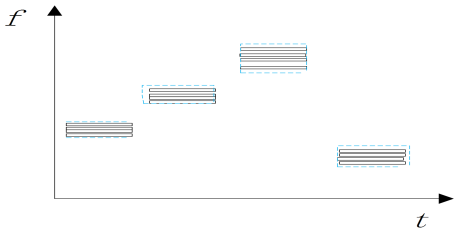


**FIGURE 12.** Marking principle.

of time and frequency shift. Its mathematical expression can be written as:

$$\begin{aligned} Y_i(t) &= a_m g(t - iT_b) \\ &\quad \bullet \sum_{j=1}^{m} e^{j2\pi f_{(i,j)}(t-iT_b)+j\theta} + n(t) \end{aligned} \tag{36}$$

In the formula, $Y_i(t)$ is a chaotic multi-tone modulation signal; $a_m$ is the signal amplitude and $T_b$ is the symbol time; $f_{(i,j)}, j = 1, 2, \cdots m$ is the multi-tone rate in the *ith* symbol time; $\theta$ is the random phase; $n(t)$ is the additive white Gaussian noise. Since $Y_i(t)$ is a multi-tone signal in channelized time-sharing, it is not necessary to distinguish each single tone signal, but to distinguish different $Y_i(t)$. In other words, only one of $f_k, f_k \in \{f_j, j = 1, 2, 3 \cdots m\}$ needs to be detected in the same frequency-hopping time. To suppress the cross-terms, we carry out the non-linear time-frequency analysis. After PWVD transformation, it can be expressed as:

$$PWVD_s(t,f) = \int_{-\infty}^{\infty} Y_i\left(t+\frac{\tau}{2}\right) Y_i^*\left(t-\frac{\tau}{2}\right) h(\tau)\, e^{-j2\pi f\tau} d\tau \tag{37}$$

Thus, the binarization method is applied to the time-frequency data and the background noise is removed by using its texture features then the connected region is marked. The schematic diagram of the marking principle is shown in FIGURE.12.

A heuristic method based on nearest neighbor rule is used to cluster the duration and occurrence time of the connected region thus the edge data of the connected region are calculated. The operation steps of channel identification are listed below:

1. The data of PWVD time-frequency operation are binaries, and the binarization algorithm can be referred to in the paper [34].
2. Traversing the whole time-frequency graph to remove noise-like areas in the connected domain.
3. Obtain the boundary information of the remaining connected region as shown in the border section of FIGURE.12. Cluster analysis of the boundary information is carried out to determine whether there is an effective signal in the connected region.
4. The initial channelized data can be obtained by matching the boundary information with the frequency points corresponding to the time-frequency data.

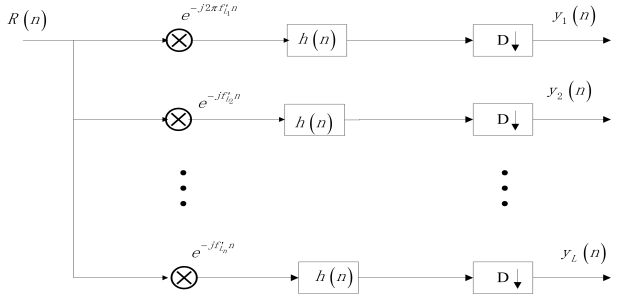


**FIGURE 13.** Principle Diagram of Channelization Processing.

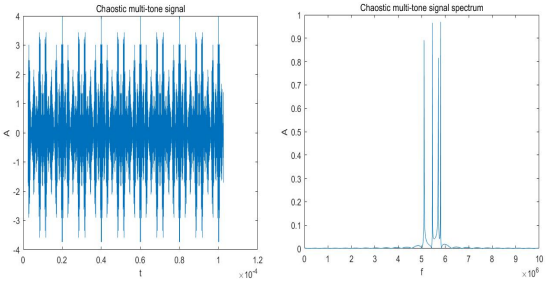


**FIGURE 14.** Waveform of the signal.

5. According to the channel division calculated in step 4, conduct a rough spectrum analysis to determine whether the frequency point interval in the adjacent windowed signal satisfies the channel interval after adding windows to the signal. If so, the channel to which the currently measured frequency point belongs is taken as the corresponding channel, and the channel frequency measured in the time-frequency diagram is denoted as: $f_h(1), f_h(2), \ldots, f_h(n)$.

#### 7) CHANNELIZED RECEIVER DESIGN

After complete the effective channelization recognition, the receiver uses matched filtering to channelize the sampled signal according to the result of signal recognition. The channelized processing module is designed as shown in FIGURE.13. Where $f'_{L_k}, 0 \le k \le L-1$ is the local signal frequency of the $kth$ channel and $L$ is the number of channels. Assuming that the down-converted signal enters a band-pass filter $h(n)$ with $B_f = f'_H - f'_L$ bandwidth. While $f'_H - f'_L = X$Hz, the frequency of the $kth$ channel is $f_{L_k} = f_h(k) - f'_L$.

For simplicity, we extract the signal by down-conversion and channelization. The decimation multiple is set $D$ here.

After that the symbol information transmitted by channel can be obtained by using chaotic multi-tone demodulation algorithm.

## V. SIMULATION VERIFICATION AND SYSTEM PERFORMANCE ANALYSIS

### A. SIMULATION OF CHAOTIC MULTI-TONE COVERT COMMUNICATION SYSTEM

In order to evaluate the performance of chaotic multi-tone covert communication system, we built a dynamic simulation system by Matlab according to the structure of transmitter and receiver. The specific implementation steps are given as follows:

1. Baseband binary data is generated by PN sequence generator. The symbol rate is $R_s = 10ksps$, the number of symbols is 14 000. These symbols are arranged in matrix form as $100 \times 140$ for chaotic scrambling. Assuming the initial value is $x_0 = 0.6, \mu = 3.6$, we can obtain the chaotic real value generated by formula (2) satisfy the chaotic scrambling rule $f[x(i)], i = 1, 2, 3 \cdots 14000$. Accordingly, the symbol matrix is scrambled by ranking quantization method.
2. The scrambled data is coded in the way of (7,4,1). Group frame processing is carried out according to the frame format in FIGURE.8. Pilot signals with a frequency range 2MHz-2.5MHz are inserted into the leading code. In order to reduce the amount of data computation, the base band frequency range of the multi-tone frequency group was set as 5MHz-10MHz. According to the method, discrete chaotic sequences were obtained to map the base band data into chaotic multi-tone signals. Each multi-tone frequency group contains four single tones. The frequency band of high frequency carrier is $f_c = 400$MHz, which is generated by amplitude modulation. The sampling rate of the system is $f_s = 2000$MHz. For simplicity, the additive white Gaussian noise is used to simulate the channel environment. FIGURE.14 shows the baseband time and frequency domain waveforms of the signal.
3. The receiver first moves the carrier by down-conversion and then filter out the interference signal and out-of-band noise with band-pass filter. The local carrier frequency $f_0 = 350$MHz is used for down conversion and the range of the band-pass filter is 55MHz-60MHz. Synchronized pilot signals are correlated with received signals by local up-sweep and down-sweep signals to obtain time delay estimation. Subsequently complete channelization and spectrum analysis according to the results of further channel recognition. When the sampling frequency is $f'_s = \frac{f_s}{10} = 200$MHz and SNR $= -5$dB. The time-frequency diagram obtained from the analysis is shown in FIGURE 15.
4. When the channelized sub-channel bandwidth is 1MHz, the sampling frequency decreases to 20MHz after extraction. FIGURE.16 is the FFT spectrum in a channel with the signal-to-noise ratio is 5dB; FIGURE.17 is the FFT spectrum in the channel with the signal-to-noise ratio is $-5$dB. The marked spectrum is the effective frequency point detected by the multi-tone demodulation algorithm.
5. As shown in FIGURE.16 and FIGURE.17, the change of noise in the channel has an impact on the amplitude of the corresponding frequency points, but has a weak influence on the final spectrum recognition results. The marked line is a multi-tone solution where effective frequency detected by the demodulation algorithm.

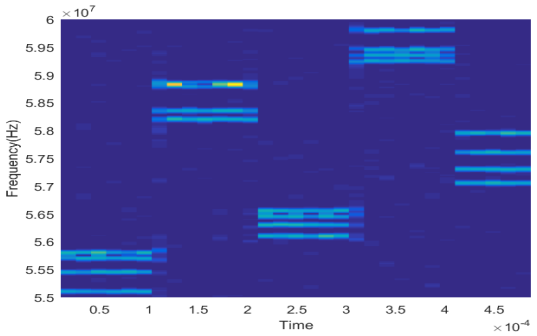


**FIGURE 15.** Signal time-frequency diagram.

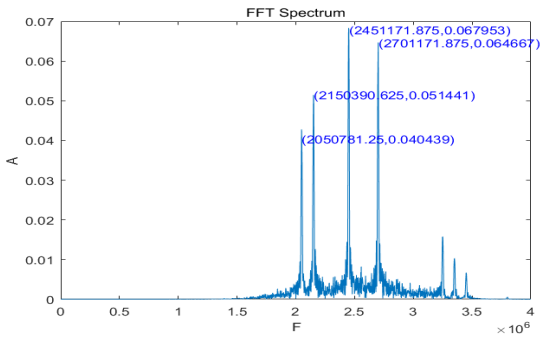


**FIGURE 16.** Effective frequency point when SNR=5dB.

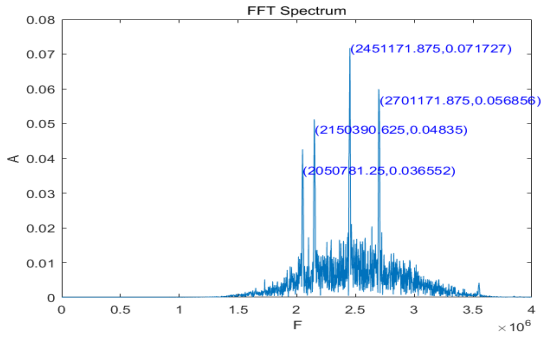


**FIGURE 17.** Effective frequency point when SNR= −5dB.

The average of the corresponding frequency points of the spectral lines in FIGURE.16 and FIGURE.17 is $\overline{f}$ while the channel center frequency is 2.5MHz. According to formula (20), the baseband data corresponding to the multi-frequency group can be obtained. If $\overline{f} \geq 2.5\text{MHz}$, $d = 1$; $\overline{f} < 2.5\text{MHz}$, $d = 0$. $d$ is baseband data.

6. Repeat step 4 and 5 until the whole frame signal is demodulated. The demodulated data should be decoded first and then the baseband data can be recovered by chaotic inversion.

### B. PERFORMANCE ANALYSIS OF CHAOTIC MULTI-TONE COVERT COMMUNICATION SYSTEM

Due to the initial value sensitivity of chaotic systems, discrete chaotic mapping sequences generated by different initial values are also different. As a result it will affect the amplitude and frequency distribution of signals in chaotic polyphonic covert communication systems. In order to visualize the signal concealment, we simulate the complex envelope amplitude and frequency distribution histogram of the signal with different initial values in FIGURE.18 and FIGURE.19.

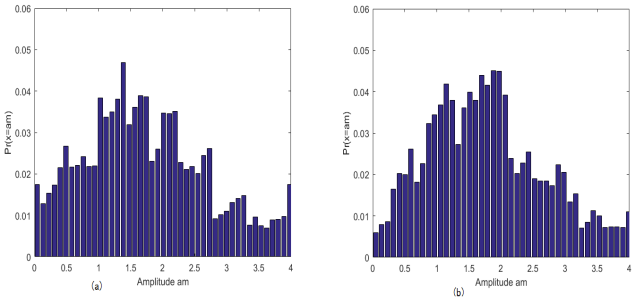


**FIGURE 18.** Complex envelope amplitude distribution histogram.

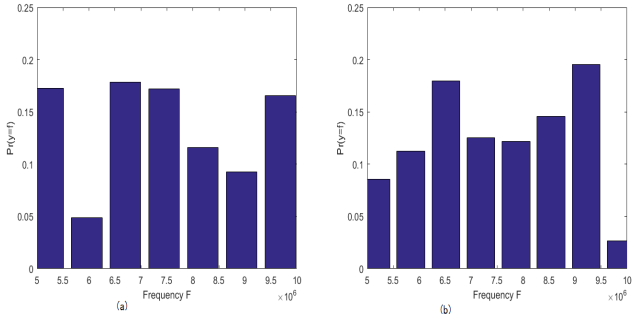


**FIGURE 19.** Frequency distribution histogram.

Since not every frequency point is employed in the broadband signal, the frequency distribution histogram cannot strictly meet the uniform distribution. However it can be seen from the in FIGURE.18 and FIGURE.19 that there is frequency division multiplexing in the system. Furthermore, it can achieve the purpose of covert communication and anti-interception while the envelope amplitude and frequency distribution corresponding to each frame signal are different. Therefore, the non-cooperative party cannot observe the modulation mode by the information such as amplitude or frequencies when it unable to intercept all chaotic multi-tones (i.e. multi-tone rate combination A and B). So this modulation method has excellent anti-interception and anti-demodulation performance.

The curve shown in FIGURE.20 illustrates the comparison of bit error rates between the non-cooperative receiver and the cooperative receiver. The goal of the non-cooperative receiver is to detect the transmissions by using the broadband receiver. Two scenarios are assumed here: 1-non-cooperative user captures the effective signal and analyzes the multi-tone frequency group within each symbol time, but the corresponding relationship between chaotic multi-tone frequency group and baseband symbol is not clear and attempts to decode other relations; 2-the non-co-user has

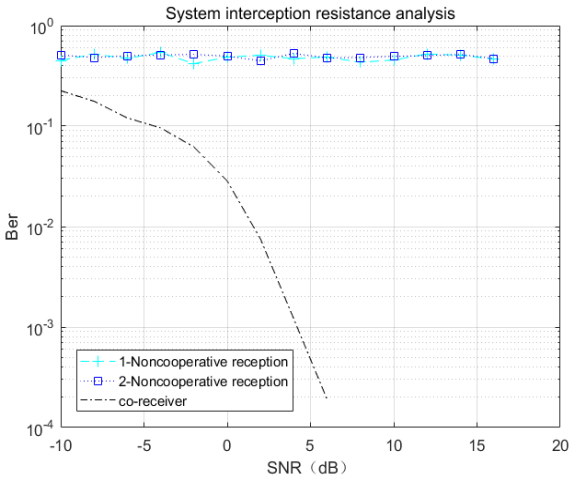


**FIGURE 20.** System interception resistance analysis.

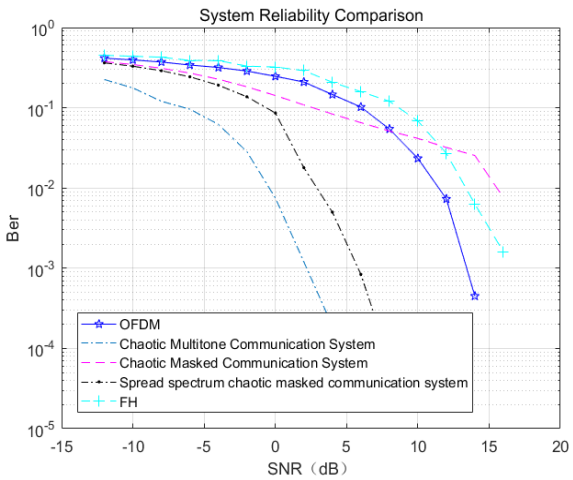


**FIGURE 21.** System BER curve.

further deciphered the correspondence between the multi-tone frequency group and the baseband symbol, but is ignorant of the symbol chaos scrambling rule. According to FIGURE.20, when the non-cooperative user cannot fully understand the chaotic multi-tone demodulation scheme and the corresponding scrambling rules, the bit error rate of the receiver maintains between 0.4-0.5, indicating that the non-cooperative party cannot demodulate useful information. To decode the scrambling rule accurately, it is equivalent to decoding the parameters of the chaotic system. According to the literature [37], only when the estimation error of the initial value is less than $10^{-20}$ for chaotic scrambling mode, can the non-cooperator decode the signal completely and this cost is very large.

In this chaotic multi-tone covert communication system, the signal demodulation is implemented based on the decision result of the multi-spectral lines. It is difficult to determine its performance by qualitative analysis because the single spectral line recognition error or multi-tone interference would not affect the decision results necessarily. Therefore, we verifiy the anti-jamming ability of the system through Monte Carlo experiment, and compares it with OFDM communication system, conventional chaotic masking communication system, spread spectrum communication system and frequency hopping communication system. In the same white Gaussian noise environment, the BER curves of the systems obtained by simulation are shown in FIGURE.21.

As shown in FIGURE.21, except for the conventional chaotic masked communication system, the other three communication systems adopt spread spectrum mode to improve the reliability of the system. In this system, the processing gain is $G = {}^{B_w}/_{R_b}$. In order to facilitate the comparison, the spread spectrum chaotic masking system has the same processing gain with the chaotic multi-tone communication system. The result demonstrate that the propose system achieves 3.5dB over the spread spectrum chaotic masking system at the BER of $10^{-3}$. Obviously, due to the error redundancy of the multi-tone modulation method and the coding gain, the system is superior to the conventional spread spectrum chaotic communication system. The OFDM and the FH system has the same $B_w$ with the chaotic multi-tone communication system while the $R_b$ of our system is lower than OFDM system. However the proposed system in this paper have the higher processing gain. Compared with the OFDM system the additional processing gain can be converted to dB as 10dB. As we can see from the BER comparison curve achieves 12dB over the OFDM system at the BER of $10^{-3}$ due to the higher processing gain and the the coding gain. In other words, compared with OFDM systems, our proposed method achieves better reliability at the expense of limited spectrum resources.

There are different frequency point combination modes in the same channel which indicates that the signal has the form of frequency point multiplexing. Different from the OFDM system, the signal does not need to satisfy the orthogonality to complete frequency division multiplexing. Therefore, the system has more space to improve the spectrum efficiency and its reliability is higher than FH and chaotic communication system.

The above performance comparisons is implemented over Additive White Gaussian Noise (AWGN) channel. For tackling the practicability of the proposed system in wireless mobile channel, we analyze the performance over the multi-path fading channels. Inspired by the theory in papaer [38]–[40], Nakagami-m fading appears to be a more generalized distribution by which a myriad of fading environments can be accurately characterised. Note that the chaotic multi-tone convert communication system employ the Multi-carrier transmission technology, we now compare the error performance of the propose the scheme in the paper with the OFDM communication system, spread spectrum communication system and frequency hopping communication system. Base on the paper [41], the fading depth $m$ represents the type of fading while convert communication mainly take care of the slow fading. For the sake of the fairness in the experiments the fading depth $m = 2$. FIGURE.22 shows the BER results

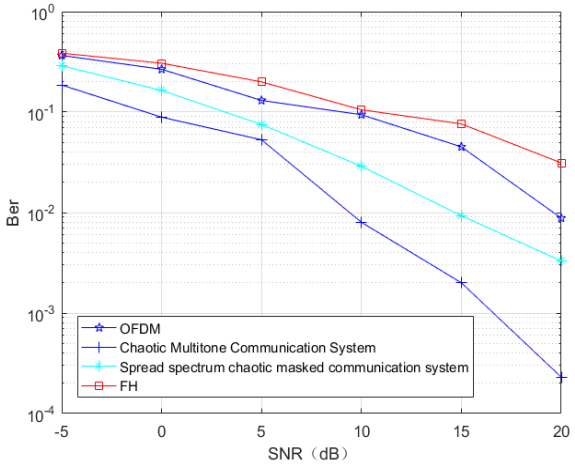


**FIGURE 22. BER comparison over a multi-path Nakagami fading channel with fading depth $m = 2$.**

of the system over a multi-path Nakagami fading channel with fading depth $m = 2$.

Referring to FIGURE.22, the chaotic multi-tone convert communication system achieves 4.8dB over the spread spectrum communication system with the same processing gain, which is 1.3dB higher than the performance of AWGN channel. In summary, the proposed scheme has the ability to resist the multi-path channel fading with the advantage of Multi-carrier transmission technology.

## VI. CONCLUSION

In this paper we propose a new method of information confrontation in modulation mode and illustrated an algorithm of mapping between discrete sequence and multi-frequency group in accordance with chaotic law. Moreover, we not only bring out the One-to-many mapping of baseband code, but also implements the concrete design scheme and key technology realization of chaotic multi-tone covert communication system. The performance of transmitter and receiver of the system is verified on Matlab simulation platform. Accordingly, we put forth the bit error rate analysis of signals under different SNR ratio over AWGN and multi-path channel fading channels. The simulation results show that the system has good anti-noise performance at low signal-to-noise ratio. However the algorithm in this paper is only used to transmit binary symbols. The frequency band utilization and the information carrying capacity of signals are needed to be improved. On the other hand, the mathematical algorithm of mapping between baseband codes and multi-audio rates tends to be less diversified. The next step is to improve the bandwidth utilization of the system and design more difficult to decipher the mathematical mapping algorithm to improve the concealment of signal modulation and demodulation mode.

## REFERENCES

[1] M. A. Landolsi, "Novel signals for optimized timing synchronization in direct-sequence spread-spectrum communication systems," *Int. J. Commun. Syst.*, vol. 31, no. 14, 2018, Art. no. e3735.

[2] S.-H. Lee, L. Wang, A. Khisti, and G. W. Wornell, "Covert communication with channel-state information at the transmitter," *IEEE Trans. Inf. Forensics Security*, vol. 13, no. 9, pp. 2310–2319, Sep. 2018.

[3] L. Wang, G. W. Wornell, and L. Zheng, "Fundamental limits of communication with low probability of detection," *IEEE Trans. Inf. Theory*, vol. 62, no. 6, pp. 3493–3503, Jun. 2016.

[4] A. Kaveh and S. M. Javadi, "Chaos-based firefly algorithms for optimization of cyclically large-size braced steel domes with multiple frequency constraints," *Comput. Struct.*, vol. 214, pp. 28–39, Apr. 2019.

[5] G. Sangirov, Y. Fu, J. Sangirov, and A. Olmasov, "Performance enhancement in LDPC coded high-dimension MIMO-OFDM systems," in *Proc. 2nd Int. Conf. Electron., Netw. Comput. Eng. (ICENCE)*, Sep. 2016, pp. 455–460.

[6] Z. Mihret and M. W. Ahmad, "The reverse engineering of reverse encryption algorithm and a systematic comparison to DES," *Procedia Comput. Sci.*, vol. 85, pp. 558–570, May 2016.

[7] B. Ning, L. Guan, and H. Huang, "A novel frequency-hopping sequence for covert communication," *IEEE Access*, vol. 5, pp. 20157–20163, 2017.

[8] N. S. Cao, J. Zhao, and Y. Q. Ding, "Realization and improvement of navigation function of link16," *Telecommun. Eng.*, vol. 51, no. 5, pp. 6–11, May 2011.

[9] J. Choi, "Physical layer security for channel-aware random access with opportunistic jamming," *IEEE Trans. Inf. Forensics Security*, vol. 12, no. 11, pp. 2699–2711, Nov. 2017.

[10] Y. Fu, X. Li, Y. Li, W. Yang, and H. Song, "Chaos M-ary modulation and demodulation method based on Hamilton oscillator and its application in communication," *Chaos*, vol. 23, no. 1, 2013, Art. no. 013111.

[11] H. R. Azarboni, R. Ansari, and A. Nazarinezhad, "Chaotic dynamics and stability of functionally graded material doubly curved shallow shells," *Chaos, Solitons Fractals*, vol. 109, pp. 14–25, Apr. 2018.

[12] W. Zhang, C. Zhang, C. Chen, W. Jin, and K. Qiu, "Joint PAPR reduction and physical layer security enhancement in OFDMA-PON," *IEEE Photon. Technol. Lett.*, vol. 28, no. 9, pp. 998–1001, May 1, 2016.

[13] P. Qiu, Y. Lyu, J. Zhang, D. Wang, and G. Qu, "Control flow integrity based on lightweight encryption architecture," *IEEE Trans. Comput.-Aided Des. Integr. Circuits Syst.*, vol. 37, no. 7, pp. 1358–1369, Jul. 2018.

[14] S. Angizi, Z. He, N. Bagherzadeh, and D. Fan, "Design and evaluation of a spintronic in-memory processing platform for nonvolatile data encryption," *IEEE Trans. Comput.-Aided Design Integr.*, vol. 37, no. 9, pp. 1788–1801, Sep. 2018.

[15] J. Zheng, H. Hu, and X. Xia, "Applications of symbolic dynamics in counteracting the dynamical degradation of digital chaos," *Nonlinear Dyn.*, vol. 94, no. 2, pp. 1535–1546, 2018.

[16] A. Argyris, M. Boumpos, A. Bogris, and D. Syvridis, "Statistical properties of broadband chaotic signals for ultrafast true random bit sequence generation," in *Proc. 39th Eur. Conf. Exhib. Opt. Commun. (ECOC)*, Sep. 2013, pp. 1–3.

[17] G. Zhao, G. Chen, J. Fang, and G. Xu, "Block cipher design: Generalized single-use-algorithm based on chaos," *Tsinghua Sci. Technol.*, vol. 16, no. 2, pp. 194–206, 2011.

[18] M. Joshi, A. Kumar, P. Ghosh, B. P. Das, and M. Devi, "North almora fault: A crucial missing link in the strike slip tectonics of western Himalaya," *J. Asian Earth Sci.*, vol. 172, pp. 249–263, Apr. 2019.

[19] C. You, I. Kim, S. Han, J. Jeong, and D. Kim, "Performance improvement of ranging and communication system using ultra wide-band tilted frequency chirp signal," in *Advances in Computer, Communication, Control and Automation*, vol. 121. 2011, pp. 313–320.

[20] T. Wu, J. Luo, J. Fang, J. Ma, and X. Song, "Unsupervised object-based change detection via a Weibull mixture model-based binarization for high-resolution remote sensing images," *IEEE Geosci. Remote Sens. Lett.*, vol. 15, no. 1, pp. 63–67, Jan. 2018.

[21] V. C. Chen and H. Ling, "Joint time-frequency analysis for radar signal and image processing," *IEEE Signal Process. Mag.*, vol. 16, no. 2, pp. 81–93, Mar. 1999.

[22] S. Shao, D. Liu, K. Deng, Z. Pan, and Y. Tang, "Analysis of carrier utilization in full-duplex cellular networks by dividing the co-channel interference region," *IEEE Commun. Lett.*, vol. 18, no. 6, pp. 1043–1046, Jun. 2014.

[23] J. I. Tello and M. Winkler, "Stabilization in a two-species chemotaxis system with a logistic source," *Nonlinearity*, vol. 25, no. 5, pp. 1413–1425, 2012.

[24] K. J. Persohn and R. Povinelli, "Analyzing logistic map pseudorandom number generators for periodicity induced by finite precision floating-point representation," *Chaos Solitons Fractals*, vol. 45, no. 3, pp. 238–245, 2012.
[25] P. Chen, Y. Fang, K. Su, and G. Chen, "Design of a capacity-approaching chaos-based multiaccess transmission system," *IEEE Trans. Veh. Technol.*, vol. 66, no. 12, pp. 10806–10816, Dec. 2017.
[26] L. Sui, K. Duan, J. Liang, and X. Hei, "Asymmetric double-image encryption based on cascaded discrete fractional random transform and logistic maps," *Opt. Express*, vol. 22, no. 9, pp. 10605–10621, 2014.
[27] S. M. T. Nezhad, M. Nazari, and E. A. Gharavol, "A novel DoS and DDoS attacks detection algorithm using ARIMA time series model and chaotic system in computer networks," *IEEE Commun. Lett.*, vol. 20, no. 4, pp. 700–703, Apr. 2016.
[28] T. Le, X. Chen, and Y. Liu, "NCOM: Network coding based overlay multicast in wireless networks," *Wireless Netw.*, vol. 21, no. 1, pp. 187–199, 2015.
[29] S. Li, C. Ding, M. Xiong, and G. Ge, "Narrow-sense BCH codes over GF($_q$) with length $n = q(m)$-1/$q$-1," *IEEE Trans. Inf. Theory*, vol. 63, no. 11, pp. 7219–7236, Nov. 2017.
[30] D. Jo, S. Kwon, and D.-J. Shin, "Blind reconstruction of BCH codes based on consecutive roots of generator polynomials," *IEEE Commun. Lett.*, vol. 22, no. 5, pp. 894–897, May 2018.
[31] K. Xu, Y. Xu, W. Ma, W. Xie, and D. Zhang , "Time and frequency synchronization for multicarrier transmission on hexagonal time-frequency lattice," *IEEE Trans. Signal Process.*, vol. 61, no. 24, pp. 6204–6219, Dec. 2013.
[32] D. Oh, J. Lee, and J.-W. Chong, "An effective pre-filtering method with a propagator for TOA-based range estimation using chirp signal," *IEEE Commun. Lett.*, vol. 15, no. 9, pp. 929–931, Sep. 2011.
[33] K. Sun, M. Zhang, and D. Yang, "A new interference detection method based on joint hybrid time–frequency distribution for GNSS receivers," *IEEE Trans. Veh. Technol.*, vol. 65, no. 11, pp. 9057–9071, Nov. 2016.
[34] A. Ghaderi, H. A. Mohammadpour, H. L. Ginn, and Y.-J. Shin, "High-impedance fault detection in the distribution network using the time-frequency-based algorithm," *IEEE Trans. Power Del.*, vol. 30, no. 3, pp. 1260–1268, Jun. 2015.
[35] L. Dai, J. Wang, Z. Wang, P. Tsiaflakis, and M. Moonen, "Spectrum- and energy-efficient OFDM based on simultaneous multi-channel reconstruction," *IEEE Trans. Signal Process.*, vol. 61, no. 23, pp. 6047–6059, Dec. 2013.
[36] A. Kliks, D. Triantafyllopoulou, L. De Nardis, O. Holland, L. Gavrilovska, and A. Bantouna, "Cross-layer analysis in cognitive radio—Context identification and decision making aspects," *IEEE Trans. Cogn. Commun. Netw.*, vol. 1, no. 4, pp. 450–463, Dec. 2015.
[37] L. Ni and X. Da Hanghu, "Anti-interception communication based on improved logistic phase scrambling code," *J. Huazhong Univ. Sci. Technol. (Natural Sci. Ed.)*, vol. 47, no. 6, pp. 35–40, Jun. 2019.
[38] Y. Fang, G. Han, P. Chen, F. C. M. Lau, G. Chen, and L. Wang, "A survey on DCSK-based communication systems and their application to UWB scenarios," *IEEE Commun. Surveys Tuts.*, vol. 18, no. 3, pp. 1804–1837, 3rd Quart., 2016.
[39] P. Chen, L. Shi, Y. Fang, G. Cai, L. Wang, and G. Chen, "A coded DCSK modulation system over Rayleigh fading channels," *IEEE Trans. Commun.*, vol. 66, no. 9, pp. 3930–3942, Sep. 2018.
[40] Z. Du, J. Cheng, and N. C. Beaulieu, "Accurate error-rate performance analysis of OFDM on frequency-selective Nakagami-*m* fading channels," *IEEE Trans. Commun.*, vol. 54, no. 2, pp. 319–328, Feb. 2006.
[41] G. C. Alexandropoulos and K. P. Peppas, "Secrecy outage analysis over correlated composite Nakagami-*m*/gamma fading channels," *IEEE Commun. Lett.*, vol. 22, no. 1, pp. 77–80, Jan. 2018.

**YONGQING FU** received the B.S. degree in automatic control and the M.S. degree in electronic engineering from Harbin Engineering University, in 1982 and 1984, respectively, and the M.S. degree from the National University of Defense Technology, in 1985.

From October 2001 to October 2002, he was a Visiting Professor with the Department of Electrical and Computer Engineering, University of Manitoba, Canada. From January 2009 to May 2009, he was a Visiting Professor with the Department of Electrical and Computer Engineering, University of California, San Diego, CA, USA. He is currently a Professor and a Doctoral Supervisor with Harbin Engineering University. He is also a Leader of the Research Team of Radio Telemetry and Remote Control Technology. He has completed more than ten scientific research projects, published more than 120 articles, edited and published three textbooks and three monographs, and has been granted more than ten national invention patents. His research interests include weak signal detection, chaotic communication, electronic reconnaissance technology, virtual time reverse passive direction finding radar technology, and covert communication technology.

**SHENGNAN GUO** received the B.S. degree in electronic information engineering from Northeast Forestry University, in 2014. She is currently pursuing the Ph.D. degree in information and communication engineering with Harbin Engineering University. Her current research interest includes high-speed frequency-hopping signal position tracking technology.

**ZHIXIN YU** received the B.S. degree in electronic information engineering from Northeast Forestry University, in 2012, and the M.S. degree in electronic science and technology from Harbin Engineering University, in 2015, where she is currently pursuing the Ph.D. degree in information and communication engineering. Her current research interest includes virtual time reverse passive direction finding radar technology.